Journal of Combinatorial Mathematics and Combinatorial Computing
www.combinatorialpress.com/jcmcc

Combinatorial Press

Numerical Simulation Study on the Coupling Model of Groundwater Flow and Soil Deformation in Geotechnical Engineering

Xilin Yao[1, ✉]

[1] *Civil Engineering School, Wuhan University, Wuhan, Hubei, 430072, China*

ABSTRACT

This project defines and generalizes the groundwater flow and soil deformation in geotechnical engineering by combining the hydrogeological conceptual model. Based on the fluid-solid coupling theory, a coupled model of groundwater flow and soil deformation is constructed, and the SUB program package in MODFLOW simulation software is selected to numerically simulate and analyze the relationship between groundwater flow and soil deformation in the study area. In layer2 and layer3, the trend of groundwater level decline and soil compression is shown, and the other layers4~layer9 also show the same situation, due to the over-exploitation of groundwater, resulting in serious decline of the soil in the study area, which reveals the causal relationship between groundwater flow and soil deformation at present.

Keywords: fluid-solid coupling theory, groundwater flow, soil deformation, numerical simulation

1. Introduction

Geotechnical engineering is a mechanical and engineering discipline involving soil and rock bodies, which studies the mechanical properties and deformation laws of soil bodies during engineering construction and operation. In geotechnical engineering, deformation of soil body is an important research content, because it directly affects the mechanical properties of soil body and the stability of engineering structure [1-4]. The deformation of soil body can be divided into two types: elastic deformation and plastic deformation. Elastic deformation refers to the ability of the material to recover the force after being subjected to an external force, without permanent deformation. Plastic deformation refers to the permanent deformation of the material under the action of force. In geotechnical engineering, the flow of groundwater is an important influence on the deformation of the soil body [5-8].

✉ Corresponding author.
E-mail address: xilin041@gmail.com (X. Yao).

Received 03 March 2024; Revised 20 April 2024; Accepted 10 November 2024; Published Online 16 April 2025.
DOI: 10.61091/jcmcc127b-524

Groundwater flow refers to the phenomenon of groundwater flow in a geotechnical body. In geotechnical engineering, groundwater flow is a factor that is both favorable and harmful. The favorable side is the ability of groundwater to create effective loads and enhance the stability of the soil body [9-11]. In soils, the addition of a certain amount of water can improve the mechanical properties of soils, increase the shear strength of soils, and improve the stress performance of soils [12]. However, groundwater seepage may also bring some adverse effects. Soils with high water content are prone to softening, leading to deformation and destabilization of the soil body. Groundwater may also lead to subsidence, cracks or even collapse of the soil body through long-term scouring and erosion [13-16].

In this project, groundwater flow generalization and land deformation direction generalization are used to interpret the hydrogeological conceptual model at a deeper level. In the process of establishing the coupling model, it is assumed that only vertical deformation of the soil body occurs and the total stress does not change with time, and a three-dimensional coupling model of groundwater flow and soil deformation is obtained through mathematical calculus processing. A plain was selected as the study area, and according to the administrative area and topographic features, the plain was divided into three different areas, namely, pre-mountain, central and coastal plain, corresponding to areas A, B and C, respectively. Some mathematical parameters of the above hydrogeological conceptual and mathematical models were set, and then the MODFLOW module and SUB package of the groundwater simulation software GMS were used to validate the models and analyze the numerical simulation examples.

2. Coupled modeling of groundwater flow and soil deformation

2.1. Conceptual hydrogeological model

2.1.1. Groundwater flow generalization. The study area is a plain with mountains in the southwest and the sea in the northeast. Groundwater in the area is mainly in the Quaternary stratum, and the aquifer is a non-homogeneous anisotropic multilayer aquifer system. In the natural state, the pressurized water runoff in the study area is slow, and the overall flow is from southwest to northeast. There is a well-insulated clay layer between the two pressurized aquifers, which makes the groundwater flow between the two aquifers relatively independent. During the period of groundwater exploitation, the water head of the aquifer decreases sharply and a regional water level landing funnel is formed in the concentrated groundwater exploitation area, and the groundwater runs off from the periphery to the center of the water level funnel, and the water flow is in the state of unsteady flow. Temporally, the water level and flow rate of groundwater, as well as the source and sink terms of the groundwater system, change dynamically with time. Spatially, the overall groundwater in the study area is dominated by horizontal flow and supplemented by vertical flow, in accordance with Darcy's law [17-18]. Therefore, the groundwater flow in the study area can be generalized as a three-dimensional unsteady flow.

2.1.2. Generalization of soil deformation directions. According to the principle of effective stress, the decrease of pore water pressure is equal to the increase of effective stress under the assumption of constant total stress in the soil layer in the study area. Strictly speaking, the deformation of soil layers are all three-dimensional, and the calculation of soil deformation should all be calculated in accordance with the three-dimensional consolidation theory, but due to the wide range of this study, the deformation of soil layer in the horizontal direction is negligible compared to the deformation in the vertical direction, so this paper only considers the vertical deformation of soil layer and ignores the deformation of its horizontal direction, and it is considered that the compaction-drainage process of the cohesive soil is in accordance with the tai sha kei one-dimensional consolidation theory, namely The soil deformation is vertical one-dimensional.

2.2. Construction of the coupling model

2.2.1. Theory of fluid-solid coupling analysis:

1) Seepage theory. The flow rate through any section and the pressure or head at any point is the same as the real groundwater flow, and the Darcy's law of seepage is shown in Equation (1):

$$Q = kA\frac{\Delta h}{L} \tag{1}$$

In the formula:

Q - Seepage volume $/m^3 \cdot s^{-1}$.

K - Permeability coefficient $/m \cdot s^{-1}$.

A - Area of the seepage section $/m^2$.

L - Length of infiltration path $/m$.

Δh - Head difference between upstream and downstream $/m$.

Based on the principle of conservation of mass i.e. the flow into the cell is equal to the flow out of the cell and ignoring the gas transport process during stress deformation [19-21]. The soil cell is shown in Fig. 1, setting n as the porosity and q_{in} as the flow rate along the coordinate axis in the positive direction into the soil cell, and its expression equation is according to the following equation (2):

$$q_{in} = \rho\left(q_x \Delta y \Delta z + q_y \Delta x \Delta z + q_z \Delta x \Delta y\right) \tag{2}$$

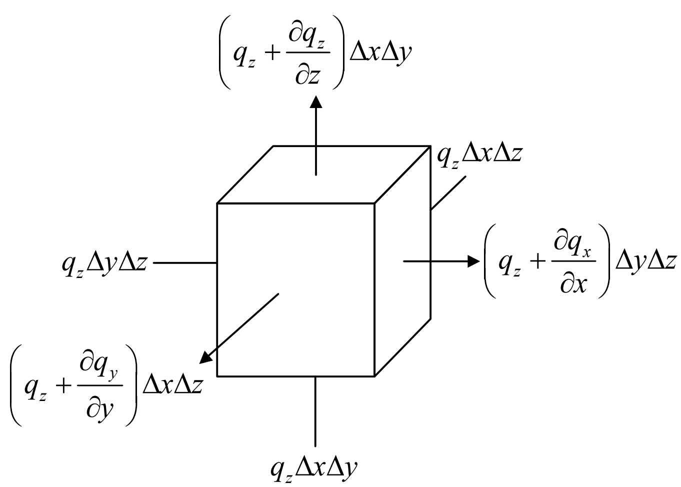

Fig. 1. Principle of liquid fluidity of soil units

The flow rate out of the soil unit is set to be q_{out}, and the expression equation is given in Eq. (3):

$$q_{out} = \rho\left[\left(q_x + \frac{\partial q_z}{\partial x}\Delta x\right)\Delta y \Delta z + \left(q_y + \frac{\partial q_y}{\partial y}\Delta y\right)\Delta x \Delta z + \left(q_z + \frac{\partial q_z}{\partial z}\Delta z\right)\Delta x \Delta y\right] \tag{3}$$

The difference between the inflow and outflow of a soil unit is defined as the recharge rate of the soil unit Δq, and the volumetric water content of the soil unit is related to the change in the recharge rate by the relationship of Equation (4):

$$\Delta q = \rho \frac{\partial \theta}{\partial t} \Delta x \Delta y \Delta z \tag{4}$$

The soil unit recharge rate Δq can also be expressed as equation (5):

$$\Delta q = q_{in} - q_{out} \tag{5}$$

Substituting Eqs. (2) to (4) into Eq. (5) yields the unsteady flow pit control equations applicable to saturated and unsaturated soils:

$$-\rho\left(\frac{\partial q_s}{\partial x} + \frac{\partial q_j}{\partial y} + \frac{\partial q_z}{\partial z}\right) = \rho \frac{\partial \theta}{\partial t} \tag{6}$$

Firstly, the soil is regarded as an isotropic pore medium with a fixed skeleton, and it is combined with Darcy's law and the continuity equation to express the infiltration rate in terms of the permeability coefficient and the hydraulic gradient, and finally the basic partial differential equation describing the water movement of unsaturated soils is derived, and its expression is according to the following equation (7):

$$\frac{\partial}{\partial x}\left(K_x \frac{\partial h}{\partial x}\right) + \frac{\partial}{\partial y}\left(K_y \frac{\partial h}{\partial y}\right) + \frac{\partial}{\partial z}\left(K_z \frac{\partial h}{\partial z}\right) = \frac{\partial \theta}{\partial t} \tag{7}$$

For the problem of two-dimensional percolation, Eq. (7) can be written as Eq. (8) below:

$$\frac{\partial}{\partial x}\left(K_x \frac{\partial h}{\partial x}\right) + \frac{\partial}{\partial z}\left(K_z \frac{\partial h}{\partial z} - K_z\right) = \frac{\partial \theta}{\partial t} \tag{8}$$

Figure 2 shows the soil-water characteristic curve. The saturation of the soil body shows a decreasing curve shape with the increase of suction, and the curve can be roughly divided into three regions, which are the boundary effect zone where the pores are filled with water, at which time the saturation decreases slightly, and the matrix suction increases slightly; the transition zone when the pore water of the soil body is discharged, and the matrix suction increases significantly with the change of the saturation degree; and the inter-particle force between the soil particles in the residual zone of the unsaturated soil is large because of the high matrix suction, which results in the The shear strength of the soil body is enhanced. When the matrix suction force is greater than 1000kPa, the saturation degree has less influence on the curve, and the curve is convergent at this time.

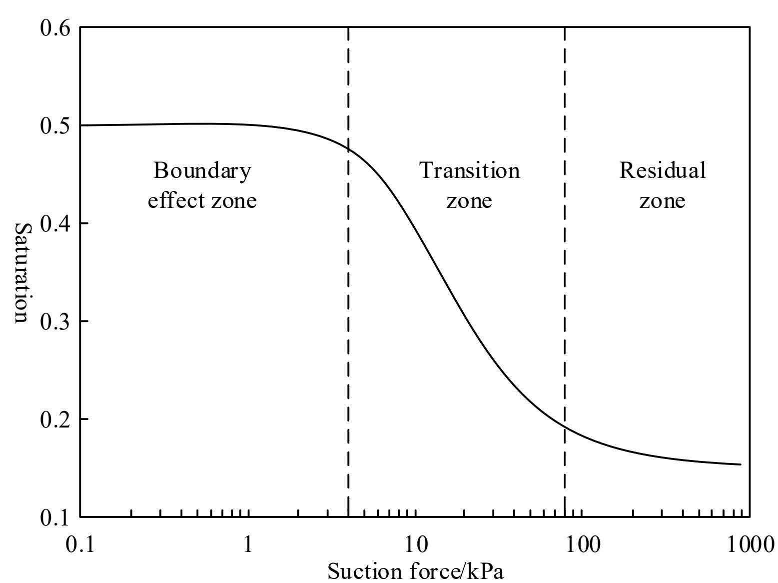

Fig. 2. Soil-water characteristic curve

When we study the saturated-unsaturated seepage problem, we need to first determine the solution condition of the seepage model, which is composed of boundary conditions and initial conditions. In general, we divide the boundary conditions into three types, the first type of boundary conditions is also known as the head boundary, that is, all the head boundaries $H_0(x,y,z)$ on this type of boundary are known:

$$H(x,y,z,t)=H_0(x,y,z)\Big|_{(x,y,z)\in s_1} \tag{9}$$

The second type of boundary condition is also known as a flow boundary, i.e., the amount of seepage per unit area on this type of boundary q is known:

$$K\frac{\partial H}{\partial n}|s_2 = q_1(x,y,z,t),(x,y,z)\in s_2 \tag{10}$$

The third type of boundary condition is the mixed boundary condition, which is the combined distribution of head and its normal derivative under certain boundary conditions i.e., constant head boundary and flow boundary conditions exist on a boundary at the same time.

2) Consolidation theory. It is well known that soil is composed of solid, liquid and gaseous three items, the volume of the soil gradually decreases under the action of external loads, and the process of pore water being gradually discharged is called soil consolidation. Continuity conditions: dt time the change of water volume within the microelement should be equal to the change of pore volume within the microelement. dt The change of water volume Q within the microelement in time is given by equation (11):

$$dQ=\frac{\partial Q}{\partial t}\cdot dt=\left[qdxdy-\left(q+\frac{\partial q}{\partial z}dz\right)dxdy\right]dt=-\frac{\partial q}{\partial z}dxdydzdt \tag{11}$$

Eq:

q - the volume of water flowing through a unit horizontal cross-sectional area per unit time.

The change in pore volume V_v within the microelement during dt time is given by Eq. (12):

$$dV_v=\frac{\partial V_v}{\partial t}dt=\frac{1}{1+e_1}\frac{\partial e}{\partial t}dxdydzdt \tag{12}$$

Eq:

e_1 - Initial pore ratio before seepage consolidation.

Obtained from $dQ=dV_v$: i.e:

$$\frac{1}{1+e_1}\cdot\frac{\partial e}{\partial t}=-\frac{\partial q}{\partial z} \tag{13}$$

Equation (14) is obtained from Darcy's law:

$$q=ki=k\frac{\partial h}{\partial z}=\frac{k}{\gamma_w}\frac{\partial u}{\partial z} \tag{14}$$

Eq:

i - Head gradient.

h - Superhydrostatic head.

u - Super pore water pressure.

According to the relationship between the change of pore ratio and the change of vertical effective stress under the side-limit condition get equation (15):

$$\frac{\partial e}{\partial t}=-\frac{a\partial\sigma'}{\partial t} \tag{15}$$

According to the effective stress principle, Eq. (15) is changed to Eq. (16):

$$\frac{\partial e}{\partial t}=-\frac{a\partial\sigma'}{\partial t}=\frac{a\partial(\sigma-u)}{\partial t}=\frac{a\partial u}{\partial t} \tag{16}$$

The above equations are pushed to apply the condition that the total vertical stress σ at any point in the one-dimensional consolidation process does not vary with time. Substituting Eq. (14) and Eq. (16) into Eq. (13) yields:

$$\frac{a}{1+e_1}\frac{\partial u}{\partial t}=\frac{k}{\gamma_w}\frac{\partial^2 u}{\partial^2 z} \tag{17}$$

Let $C_v=\frac{k\left(1+e_1\right)}{a\gamma_w}=\frac{kE_s}{\gamma_w}$, then Eq. (17) becomes the following Eq. (18) which is the Terzaghi one-dimensional consolidation differential equation, where C_v is called the vertical consolidation coefficient of the soil $\left(cm^2/s\right)$:

$$\frac{\partial u}{\partial t}=C_v\frac{\partial^2 u}{\partial^2 z} \tag{18}$$

The total stress during consolidation is assumed to be constant. The basic differential equation for 3D consolidation is Eq. (19):

$$C_{vx}\frac{\partial^2 u}{\partial x^2}+C_{vy}\frac{\partial^2 u}{\partial y^2}+C_{vz}\frac{\partial^2 u}{\partial z^2}=\frac{\partial u}{\partial t} \tag{19}$$

Eqs:

C_{vx}, C_{vy}, C_{vz} - coefficient of consolidation in x, y, z directions.

The equilibrium differential equation expressed in terms of displacement and pore water pressure is derived from the effective stress and elastic mechanics as in Eq. (20):

$$\begin{cases}-G\Delta^2 w_x-\frac{G}{1-2v}\cdot\frac{\partial}{\partial x}\left(\frac{\partial w_x}{\partial x}+\frac{\partial w_y}{\partial y}+\frac{\partial w_z}{\partial z}\right)+\frac{\partial u}{\partial x}=0\\ -G\Delta^2 w_y-\frac{G}{1-2v}\cdot\frac{\partial}{\partial y}\left(\frac{\partial w_x}{\partial x}+\frac{\partial w_y}{\partial y}+\frac{\partial w_z}{\partial z}\right)+\frac{\partial u}{\partial y}=0\\ -G\Delta^2 w_z-\frac{G}{1-2v}\cdot\frac{\partial}{\partial z}\left(\frac{\partial w_x}{\partial x}+\frac{\partial w_y}{\partial y}+\frac{\partial w_z}{\partial z}\right)+\frac{\partial u}{\partial z}=0\end{cases} \tag{20}$$

Eq:

Δ^2 - Laplace operator.

The above Eq. (20) has three equations, but includes four unknown quantities respectively: w_x, w_y, w_z three displacements and pore water pressure u, so it is necessary to add another continuity equation. From Darcy's law, the unit flow rate through the tiny soil bodies x, y, and z on the surface is Eq. (21), respectively:

$$\begin{cases} q_x = -\dfrac{K_x}{\gamma_y}\dfrac{\partial u}{\partial x} \\ q_y = -\dfrac{K_y}{\gamma_z}\dfrac{\partial u}{\partial y} \\ q_z = -\dfrac{K_z}{\gamma_z}\dfrac{\partial u}{\partial z} \end{cases} \tag{21}$$

Eq:
K_x, K_y, K_z - coefficient of permeability in three directions.
γ_w - the capacitive weight of water.
From the continuity of saturated soil, it is known that the unit time unit soil compression should be equal to the sum of the changes in the flow rate across the surface of the unit, that is, Equation (22):

$$\frac{\partial}{\partial t}\left(\varepsilon_y dxdydz\right) = \frac{\partial\left(q_x dydz\right)}{\partial x}dx + \frac{\partial\left(q_y dxdz\right)}{\partial y} + \frac{\partial\left(q_z dxdy\right)}{\partial z} \tag{22}$$

Substituting Eq. (21) and expressing ε_v in terms of displacement, the above equation can be simplified to:

$$\frac{\partial}{\partial t}\left(\frac{\partial w_x}{\partial x} + \frac{\partial w_x}{\partial y} + \frac{\partial w_z}{\partial z}\right) = \frac{K_x}{\gamma_x}\frac{\partial^2 u}{\partial x} + \frac{K_y}{\gamma_x}\frac{\partial^2 u}{\partial y} + \frac{K_z}{\gamma_w}\frac{\partial^2 u}{\partial z} \tag{23}$$

The above equation (23) is the continuity equation expressed in terms of pore water pressure and displacement, and the Biot consolidation equation is derived by coupling the equilibrium equation (20) with the continuity equation (23).

3) Fluid-solid coupling theory. The fluid-solid coupling theory mainly studies the mechanical properties of deformable solids in the infiltration process and their influence on the seepage field, and in this way reveals the relationship between fluid and solid interaction. In MODFLOW software, it is firstly assumed that the seepage of liquid in pore medium conforms to Darcy's law, from which the continuity equation of seepage of liquid in pore medium can be derived, specifically as in Equation (24):

$$\begin{cases} \dfrac{\partial}{\partial t}\left(\varepsilon_p \rho_f\right) + \nabla\left(\rho_f u\right) = Q_m \\ \dfrac{\partial}{\partial t}\left(\varepsilon_p \rho_f\right) = \rho_f s \dfrac{\partial p}{\partial t} \\ S = \varepsilon_p \chi_f \\ u = -\dfrac{k}{\mu}\nabla p \end{cases} \tag{24}$$

Eq:
ε_p - Pore gland ratio.
ρ_f - Fluid density $kg \cdot m^{-3}$.
μ - Dynamic viscosity $/Pa \cdot s$.
Q_m - Mass source term.
S - Water storage coefficient.
x_f - Fluid viscosity coefficient $/1 \cdot Pa^{-1}$.
k - Permeability coefficient $/m \cdot s^{-1}$.
Equation (24) expresses the relationship between fluid flow in porous media and the porosity and permeability coefficient of the porous medium, which is known to obey the universal conservation law

for fluids in porous media. Therefore, the MODFLOW software relates the water pressure to the solid body strain, allowing the hydraulic properties of the fluid to vary with time under saturated-unsaturated conditions, and its equation is shown in Eq. (25):

$$\rho_f S \frac{\partial H}{\partial t} + \nabla\left(\rho_f u\right) = Q_m - \rho_f \alpha_s \frac{\partial}{\partial t} \varepsilon_{vol} \tag{25}$$

Eq:
H - Head $/m$;
α_B - Biot consolidation factor.
ε_{vol} - body strain.
The intrinsic relationship of solid pores about stress, strain and pore pressure in porous materials in MODFLOW software is shown in Eq. (26):

$$\begin{cases} \sigma = D\varepsilon_{vol} - \alpha_B P_f E \\ -\nabla \cdot \sigma = \rho_{ad} g = g\left(\rho_f \varepsilon_p + \rho_d\right) \\ P_f = \left(\zeta - \alpha_B \varepsilon_{vol}\right)/S \end{cases} \tag{26}$$

Eq:
D - elastic matrix.
P_f - Pore water pressure/Mpa.
E - Unit matrix.
ρ_{av} - Average density $/kg \cdot m^{-3}$.
ρ_d - Solid density $/kg \cdot m^{-3}$.
ζ - Value of flow change in porous pores.
The expression in the MODFLOW software for the change in volume of solids is shown in Equation (27):

$$\begin{cases} P_m = -K_s \varepsilon_{vol} + \alpha_B P_f \\ P_m = -trace(\sigma)/3 \end{cases} \tag{27}$$

From the above, it can be seen that P, ε_{vol} and Q_m at the same moment in the fluid domain of the MODFLOW software are variables, and the relationship between the parameters can be known from Eq. (24), and then the equation is substituted into Eq. (25) to derive the relationship between the changes of Q_m and ε_{vol} on the head H; P_f, ε_{vol} and σ at the same moment in the solid domain are variables, and the relationship of stress tensor on the pore strain and flow rate changes can be known from Eq. (26), and get the relationship of P_f affected by ε_{vol} and Q_m. Then, it is replaced into Eq. (27), from which the amount of change in solid volume is obtained. When proceeding to the next moment, the calculated stress tensor is coupled by calculating it as the initial pressure at the next moment.

2.2.2. Mathematical modeling. The groundwater flow in the study area is generalized to a three-dimensional unsteady flow and its three-dimensional unsteady flow differential equation can be expressed as:

$$\frac{\partial}{\partial x}\left(k_{xx}\frac{\partial h}{\partial x}\right) + \frac{\partial}{\partial y}\left(k_{yy}\frac{\partial h}{\partial y}\right) + \frac{\partial}{\partial z}\left(k_{zz}\frac{\partial h}{\partial z}\right) - W = S_s \frac{\partial h}{\partial t} \tag{28}$$

Where: k_{nz}, k_{yy}, k_{zz} represents the permeability coefficient in the main direction of the x, y, z-axis, assuming that the direction of the main axis of the permeability coefficient is the same as the direction of the coordinate axis; W is the source-sink term, h is the head value, S_s is the water storage rate, t is time.

The expression on the right side of equation (28) describes the amount of water discharged from or entered into a unit volume of water-containing medium in a unit of time, i.e., the amount of storage change. In this paper, the amount of change in storage per unit is divided into two parts: the amount of change in storage in the entrained layer and the amount of change in storage in the aquifer other than the entrained layer. Assuming that the volume percentage of the entrained layer in the aquifer system is γ , the right side of Eq. (28) should be multiplied by a factor of $(1-\gamma)$, which becomes $(1-\gamma)S_s\frac{\partial h}{\partial t}$. For a non-delayed entrained layer, the volume change of storage per unit volume is:

$$\bar{q} = \gamma S'_{sk}\frac{\partial h}{\partial t} \tag{29}$$

where S'_{sk} is the water storage rate of the interlayer skeleton, and for delayed interlayers, the change in storage per unit volume $\bar{q}$ is calculated mainly based on Darcy's law. The amount of change in storage per unit volume $\bar{q}$ is added to Eq. (28) as a right-end term to realize the coupling of the groundwater flow model and the soil deformation model. Intercalation volume change $\bar{q}$ is added to the source-sink term W in the calculation:

$$\begin{aligned}&\frac{\partial}{\partial x}\left(k_{xx}\frac{\partial h}{\partial x}\right)+\frac{\partial}{\partial y}\left(k_{yy}\frac{\partial h}{\partial y}\right)+\frac{\partial}{\partial z}\left(k_{zz}\frac{\partial h}{\partial z}\right)-(W+\bar{q})\\&=(1-\gamma)S_s\frac{\partial h}{\partial t}\end{aligned} \tag{30}$$

In the process of establishing the coupling model, it is assumed that only vertical deformation of the soil body occurs, and the total stress does not change with time, therefore, the ground settlement coupling model established in this paper is a partial coupling model. Strictly speaking, the ground settlement caused by groundwater mining is three-dimensional, and the total stress changes with time, so the partial coupling model is not perfect in terms of mechanical mechanism. However, considering the large simulation range, the deformation in the horizontal direction of the soil layer is negligible compared with the deformation in the vertical direction, and the fully coupled model requires too many parameters, the model is complicated, and can only be applied to the small-scale ground settlement simulation where the parameters are easy to obtain. Therefore, this paper establishes a partially coupled model of ground subsidence, utilizing the relationship between the water storage rate of the interlayer skeleton and the soil compression coefficient, and coupling the groundwater flow model and the soil deformation model by adding the calculated change in the interlayer storage $\bar{q}$ as a source-sink term into the water flow equation at each time period.

2.3. Simulation software selection

Based on the above hydrogeological conceptual and mathematical models, this paper uses the MODFLOW module and SUB package of the groundwater simulation software GMS (Groundwater Simulation System) to perform numerical simulation studies on the model.

2.3.1. MODFLOW groundwater modeling software. MODFLOW is a three-dimensional finite-difference numerical simulation software developed by a Geological Survey for the simulation of groundwater flow in pore media. MODFLOW adopts a modular structure, which consists of a main program and a series of highly independent subroutines to form a computer program structure. At present, many new sub-program packages have been developed, such as the SUB package for simulating ground settlement. In addition, MODFLOW has become the most widely used numerical simulation program for groundwater movement in the world because of its simple discrete method and diversified solution methods.

2.3.2. SUB settling program package. The SUB subsidence package is a ground subsidence calculation program package developed by a Geological Survey staff based on the “sandwich” theory and later coupled into MODFLOW with the same assumptions as the principle of effective stress on the tarsal base, Darcy's law, and the soil deformation equilibrium equations. The SUB package shares a main program and identical spatial and temporal discretization with MODFLOW. The SUB subsidence package and MODFLOW share the same main program and have the same spatial and temporal discretization, and any change in water level due to groundwater mining in the groundwater flow model created by MODFLOW can be reflected in the ground subsidence model created by SUB. The SUB package can be used to simulate the compression of the aquifer system due to groundwater extraction, as well as the hysteresis phenomena of discharge and compression.

3. Model Numerical Simulation Analysis

3.1. Model setup

3.1.1. Spatial Grid Segmentation. According to the hydrogeological data provided, the submerged and slightly pressurized water-bearing rock groups and the first pressurized water-bearing rock group have reached the dry state, so the study area is mainly exploited for the middle and deep groundwater, and the aquifers simulated in the numerical simulation are the second pressurized water-bearing layer and the third pressurized water-bearing layer. The simulation area is about 24.6km^2, according to the generalization of hydrogeological conditions, the study area is divided into 2 layers vertically, and the cells are divided into 100 rows and 100 columns in the plane, with a total of 20,000 cells. The outer part of the study area is invalid cells, and the other grids are cells of the model calculation range, with 41,431 valid cells and 38,519 invalid cells.

3.1.2. Time discretization. The identification simulation period is chosen as much as possible to be rich in information and close to the present time. The identification and validation period of this simulation is from November 2017 to November 2021, and the identification and validation stage is the stage of continuous decline of groundwater level and gradual formation of local landing funnel in the study area according to the provided hydrogeological conditions. The model takes one month as a stress period, which is divided into a total of 60 stress periods, and each stress period is divided into 3 time steps, totaling 180 time steps. It should be noted that the number of program iterations needs to be limited so that the model calculations automatically stop when they reach the specified number of iterations.

3.1.3. Treatment of solution conditions. The processing of the solution conditions is mainly divided into the initial conditions and boundary conditions, based on the groundwater level data in August 2017, the initial flow field of the simulated aquifer is obtained by using the Kriging interpolation method, there is no clear water separation layer between the two simulated layers and they are all pressurized aquifers, so it can be regarded as the same initial flow field of the two simulated layers, and the initial flow field of the simulated aquifer is shown in Fig. 3. This initial water head is also used as the pre-consolidation head value required in the ground settlement SUB software package. From the figure, it can be seen that the initial water level is close to the bottom of the first confined aquifer, and the boundary conditions are treated as flow boundary and general head boundary as described in the establishment of the hydrogeological conceptual model.

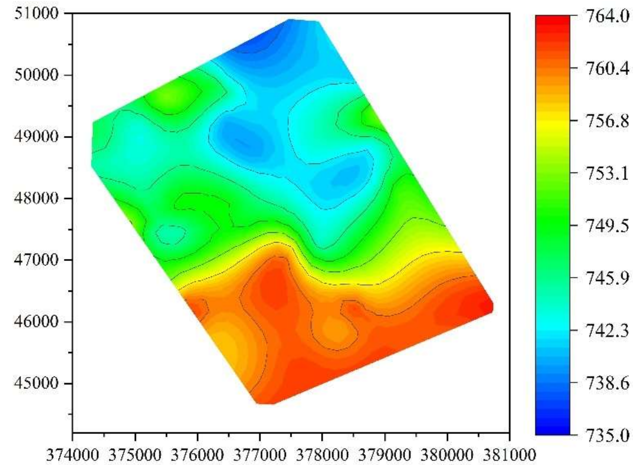

Fig. 3. Simulate initial flow field diagram of aquifer (m)

3.1.4. Hydrogeological parameterization. After constant rate determination of each parameter, 10 the values of aquifer parameters are shown in Table 1. The setting of hydrogeological parameters in the study area is mainly determined with reference to the relevant in-situ tests and test results in the area, and at the same time with reference to the empirical values of the relevant lithology. The model parameters are set using the method of preset parameters, and the relevant parameters are assigned to each aquifer during the initial simulation according to the previous data. During the identification and validation period of the model, the model is continuously fitted with reference to the actual situation, and each parameter is continuously corrected. Especially for the permeability coefficient and the degree of water supply, it is necessary to adjust them all the time during the model identification and validation period in order to reach close to the actual standard. The study area does not span a large area, so the soil parameters do not vary much.

Table 1. 10 This parameter specifies the aquifer

Aquifer	Horizontal permeability coefficient /(m·d-1)	Vertical permeability coefficient /(m·d-1)	Water release rate (m/1)	water supply
Layer 1 Partition 1	8	2	1.08E-05	0.3
Layer 1 Partition 2	16	2	1.08E-05	0.3
Floor 2	8	2	1.08E-05	0.3

3.1.5. Source and sink processing:

1) Source and sink treatment. Atmospheric precipitation first infiltrates into the loose layer of the Quaternary System, and part of it continues to infiltrate into the second and third pressurized water layers, which is an important form of obtaining precipitation recharge in the study area. Due to the lack of actual rainfall data in the study area, only the total rainfall value is available, now the rainfall infiltration recharge rate is set to 0.0025 m/d, which can be used to simulate the actual rainfall infiltration situation. The value was assigned to the numerical model by MODFLOW simulation and analysis software.

2) Artificial exploitation. Artificial extraction of groundwater has become the most important discharge item in the study area, which is mainly used for agricultural water, industrial water, and human and animal domestic water. Due to the lack of a clear time-series arrangement of pumping holes in the study area, the overall pumping volume in a year is roughly 15.5 million m^3. With the determination of extracting only the middle and deep groundwater, the pumping wells in the simulation identification stage are generalized to 38 wells, with a single-well pumping volume of 1,272 m^3/d, and the pumping wells are deployed in the vicinity of the Taigu East Station. The pumping wells were generalized to the GMS numerical model by MODFLOW simulation and analysis software.

3.2. Simulation analysis of water flow and soil coupling model validation

3.2.1. Validation of groundwater flow simulations. Figure 4 shows the groundwater flow field map of the simulated aquifer, in which (a) ~ (d) are the water flow field map in November 2017, the water flow field in November 2018, the water flow field in November 2019, the water flow field in November 2020, the water flow field in November 2021, and the groundwater contour in November 2021, respectively. This model identification and validation adopts a trial estimation and a calibration method, and repeatedly adjusts the parameters and certain source The model identification and validation used the trial estimation and correction method to repeatedly adjust the parameters and certain source items to achieve a more satisfactory simulation result. The identification and validation mainly follow: the simulated groundwater flow field should be basically consistent with the actual flow field, and the groundwater level contours should be similar in shape to the measured water level contours. The simulated groundwater dynamic process is similar to the actual dynamic process. Because there is no real-time monitoring data of water level in pumping wells in the study area, the monitoring data information is relatively scarce, and only through the Third Geological Engineering Survey Institute of Shanxi Province for many years on the dynamic monitoring results of groundwater information, to obtain from 2017 to the present, the rate of decline of the groundwater level is about 1.19m/a, and there is also the measured middle and deep water flow field in November 2021 for verification. From the simulation results, it can be seen that the overall water level in the study area is declining at an average rate of 1.19m/a, which is consistent with the dynamic monitoring results. In November 2017, the water level in the second pressurized aquifer has reached the top plate of the aquifer in some areas, and the medium-depth water landing funnel has been formed initially, with a funnel area of up to 3.18km^2, and the water level in the center of the funnel is buried at a depth of 48.37m. The water level in the study area will further decrease in November 2021, and the landing funnel will gradually expand outward, with a funnel area of 4.32km^2, and the water level in the center of the funnel is buried at a depth of 54.1m. The groundwater flow field in the simulation area basically coincides with the middle-depth isohydraulic line in November 2021, the water level trend is close to the real observation level, and the parameter rate has reached the optimum, so that the model simulation and identification validation results are satisfactory, and the model can be used to simulate the distribution of groundwater flow field, which provides a guarantee for the coupling with the ground subsidence model later on.

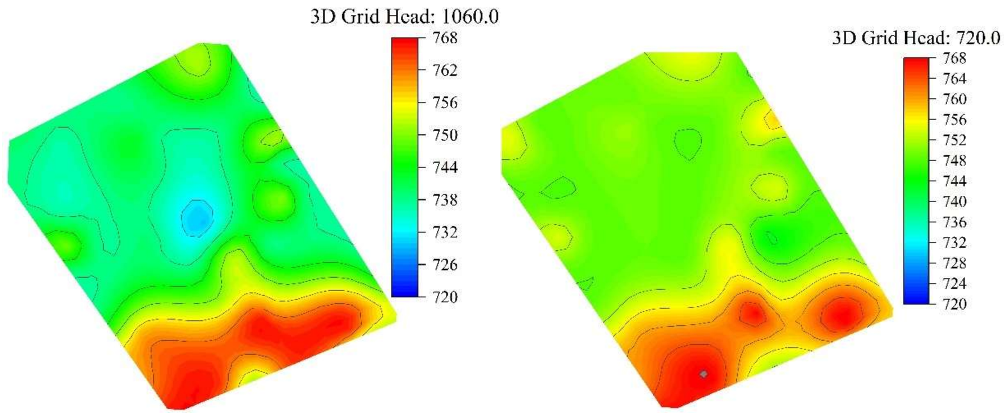

(a)Water flow field in November 2017 (b)Water flow field in November 2018

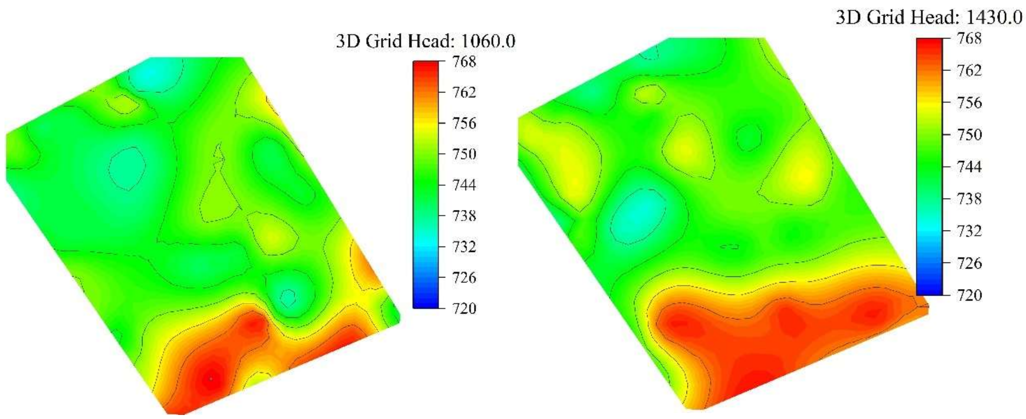

(c)Water flow field in November 2019 (d)Water flow field in November 2020

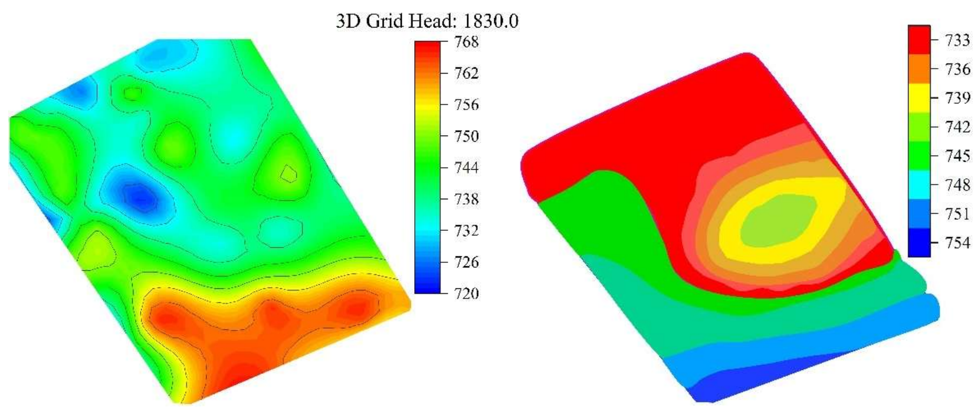

(e)Water flow field in November 2021 (f)Groundwater contours for Nov 2021

Fig. 4. Simulated aquifer groundwater flow field map (m)

3.2.2. Soil deformation model simulation analysis. Due to the lack of real-time level observation data of specific soil settlement points in the study area, the identification and validation of this soil deformation model can use the INSAR monitoring data provided by a research institute during the model identification and validation period in the study area to carry out the model identification and validation, Fig. 5 shows the simulation analysis of the soil deformation model, and the comparison of the soil deformation model identification and validation points with the InSAR monitoring values is shown in Table 2. Taking the identification and validation period of 2019.11-2021.11, it can be seen by comparison that most of the monitoring points are fitted better, and the identification effect is better, and 8 simulation points are taken to be fitted with the monitoring points, and the fitting results are better, which provides theoretical assurance for the development of the subsequent research work.

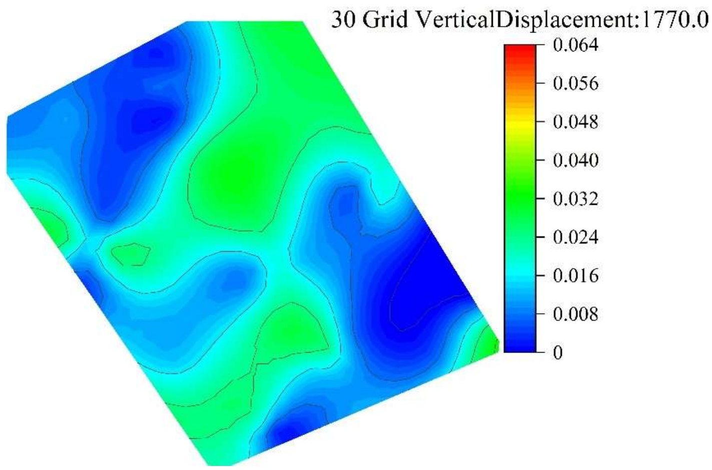

Fig. 5. Soil deformation model simulation analysis (m)

Table 2. Comparison of model identification verification points and monitoring values

N	x	y	Settlement value /mm	
			Simulated value	InSAR monitoring
1	378086	49217	-4	10~0
2	378966	48729	-16	22~-16
3	379669	47559	-9	16~-9
4	377708	47988	-13	22~-16
5	378016	47626	-24	32~-25
6	376886	47376	-12	19~-15
7	379618	46788	-3	12~-5
8	377315	47309	-16	22~-16

3.3. Groundwater flow in relation to land deformation

Through the above model validation analysis, it can be seen that the coupling model in this paper has excellent performance. In this subsection, the coupled water-soil model constructed above is used to carry out example numerical simulation analysis for typical areas A, B and C of a plain to summarize the response relationship of ground subsidence caused by groundwater exploitation in different areas. In the model, a plain is divided into three different areas, namely, mountain front, central and coastal plain, according to the administrative area and topographic features, and the relationship between groundwater flow and land deformation is investigated in areas A, B and C, respectively.

3.3.1. Analysis of groundwater flow model and land deformation model results. The mining intensity used in the model is shown in Table 3. The unsteady flow model was run by reasonably arranging the mining wells. Figures 6 to 7 represent the contour plots of the depth of groundwater level drop and the contour plots of the vertical displacement, respectively. According to the simulation results, the contour maps of groundwater level drop depth are plotted, and it can be seen that the aquifer has appeared different degrees of groundwater level landing funnels in the three areas after continuous mining for several years. The biggest degree of groundwater level descent is found in the mountain front plain area and coastal plain area, which is mainly due to the larger mining intensity in the mountain front plain area, but in Area C located in the coastal plain, although the amount of mining is not large compared to other areas, the lithology of the strata is different from that of other areas, i.e., the thickness of clay in the strata is larger, and the water-endowment condition is poor, so even if the intensity of mining is not large, it will still produce a more obvious water level descent funnel. Due to the significant decrease of groundwater level, the subsidence simulation based on the groundwater model shows that there are subsidence funnels in the central and eastern parts of the area, which are represented by areas B and C. Area C has the largest degree of subsidence, followed by area B, and there is a small amount of subsidence in area A. The pattern is that, due to the large amount of groundwater extraction in the study area, the subsidence is gradually serious from the mountain plain area to the coastal plain, and the largest subsidence funnel exists in the coastal plain. Zone C is less intensively mined than zone B but has a large degree of subsidence, reflecting the stratigraphic peculiarity of zone C, which is prone to compression.

Table 3. Mining intensity used in the model

Region	Shallow groundwater mining intensity 104m^3/(a·km^2)	Deep groundwater exploitation intensity 104m^3/(a·km^2)
A	22~16	16~9
B	12~5	16~9
C	10~0	10~0

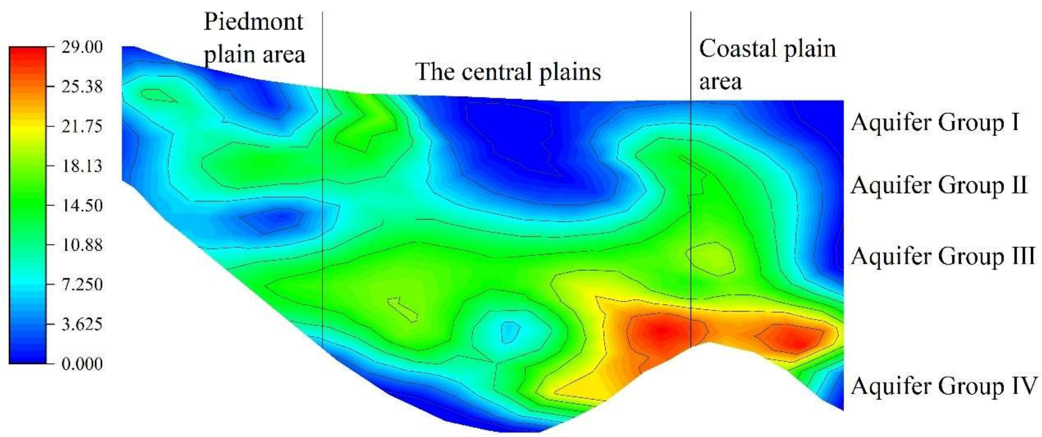

Fig. 6. Contour map of groundwater drawdown

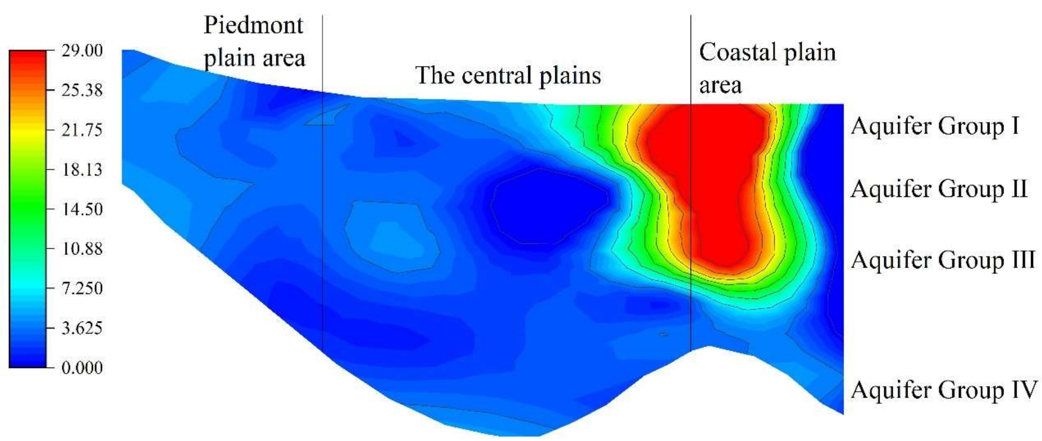

Fig. 7. Contour map of vertical displacement

According to the extraction of the grid data as shown in Table 4, the compression of each aquifer group is counted, and Fig. 8 shows the graph of the compression contribution of each aquifer group, presenting the compression contribution of each aquifer group, which shows that the compression contribution of each aquifer is different in different areas when ground subsidence occurs. By reading the graph, for the central plain area B, the ground compression is mainly provided by layers2, 3, 4, 5, and 6, i.e., aquifer group II and aquifer group III, among which aquifer group III has the largest subsidence contribution. For the stratigraphic compression in Area C of the coastal plain, the compression is mainly provided by layers 4, 5, 6, 7, 8, and 9, i.e., aquifer group III and aquifer group IV, in which aquifer group IV has the largest contribution to subsidence, followed by aquifer group III, with aquifer group II accounting for only a small amount. Since the average mining intensity in Area C is smaller than that in Hengshui, the amount of ground subsidence is much larger than that in other areas, especially the deep stratum of Area C, i.e., Aquifer Groups III and IV, is more prone to stratum compression than that in Area B.

Table 4. According to the grid data extraction

x position(km)	Compression (m)								
	layer1	Layer2	Layer3	Layer4	Layer5	Layer6	Layer7	Layer8	Laye9
0	1.71	10.32	9.54	6.28	10.84	6.24	1.58	9.88	0.59
50	1.89	18.76	17.82	12.66	27.74	11.84	3.08	16.62	0.71
100	1.7	28.1	27.84	21.83	43.95	19.58	4.85	23.27	1.31
150	1.92	41.09	42.52	33.48	59.9	27.9	6.53	27.09	1.42
200	1.89	39.91	43.37	38.94	67.46	33.92	7.72	27.97	1.79
250	1.64	36.04	42.62	46.06	78.8	43.01	9.43	30.25	2.1
300	1.76	41.03	48.58	56	90.19	51.81	10.8	29.35	2.16
350	2.12	51.86	59.16	66.04	98.38	58.02	14.52	29.71	2.75
400	2.43	48.05	59.66	78.99	119.46	75.85	22.52	40.85	4.73
450	4.79	56.07	72.82	104.16	154.66	103.77	67.01	88.07	64.74
500	6.21	76.8	98.21	144.05	206.36	142.43	148.59	248.54	244.18
550	5.37	91.94	115.81	241.36	291.03	186.47	304.09	434.7	370.62
600	2.66	61.76	73.08	130.58	130.53	74.22	144.06	92.73	10.16
650	0.27	25.76	31.37	7.46	18.73	5.34	17.86	17.04	2.53
700	1.71	10.32	9.54	6.28	10.84	6.24	1.58	9.88	0.59

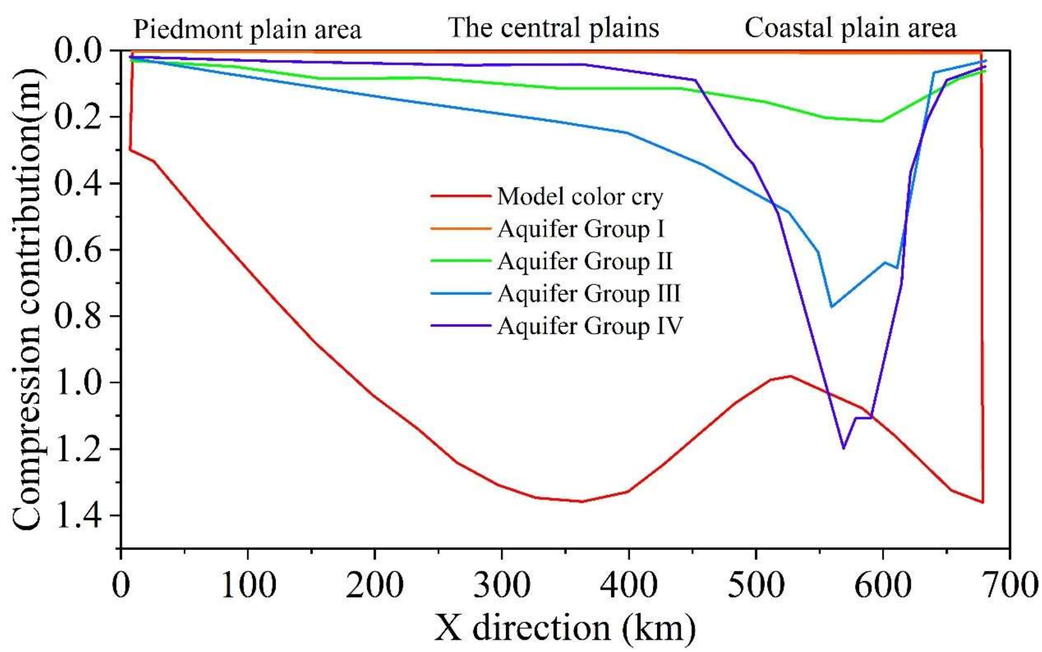

Fig. 8. Curve of compression contribution of each aquifer

The statistics of the settlement and groundwater level change of the grid in the model are plotted in Fig. 9, which shows the corresponding curves of water level change and compression in each simulated layer, where (a)~(h) represent layers2-9, respectively. Since aquifer groups II and III are pumping wells, there is a large water level drop in layers 2 and 3 and the trend of compression and water level change curves is the same. Similarly, in layer4, layer5 and layer6, the trend of water level change curve and the compression curve are the same, which indicates that the groundwater exploitation has a direct impact on the ground subsidence. There is a difference in the contribution of compression in different layers in different areas such as B and C, but compression occurs mostly in the deeper aquifers. However, in layer7, layer8 and layer9, i.e. aquifer group IV, there is no groundwater exploitation in the coastal plain area, but it also generates large changes in the groundwater level, and a large amount of ground compression is generated when the water level changes.

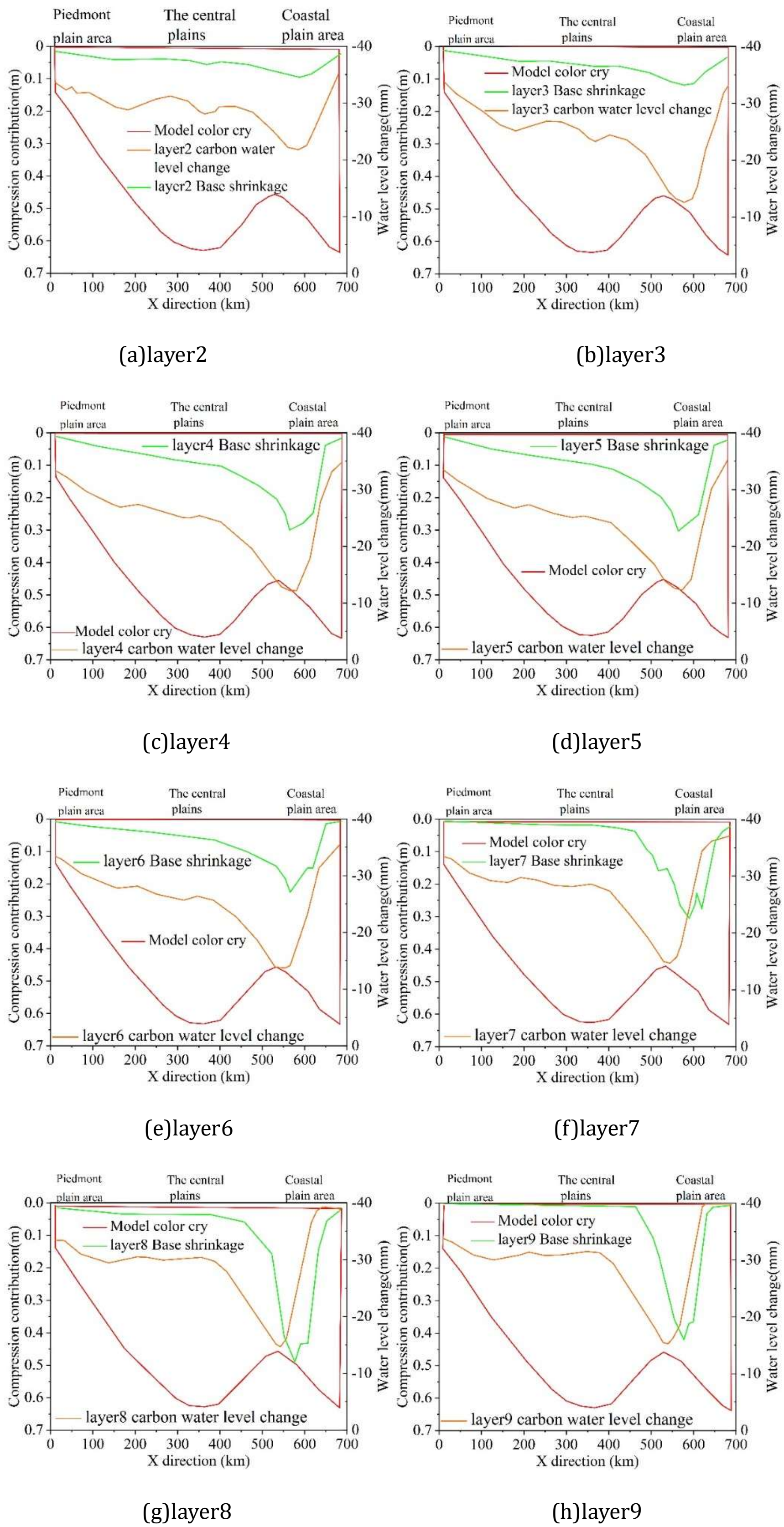

Fig. 9. Settlement and groundwater table change statistics

3.3.2. Response of ground settlement under the same mining intensity conditions. The conditions of the mining program are set as shown in Table 5, and there is a difference in the subsidence between

Area C and the Central Plains area exhibited in the above model, in order to further explore the differences in the subsidence produced under the condition of mining intensity of the same groundwater at different locations, and to consider the elimination of the disturbances caused by the inhomogeneous mining intensity.

Table 5. Mining scheme condition setting

Mining scheme	Shallow Wells	Deep well	Well flow setting
Option one	On	On	It is consistent with the mining intensity in the coastal plain area.
Option two	Off	On	It is consistent with the mining intensity in the coastal plain area

Figure 10 shows the compression volume curve of each aquifer in Scenario 1. According to the statistics of the grid information of each area in the model, the subsidence of the plain area in front of the mountain in Scenario 1 ranges from 0.001 to 0.159 m. The subsidence of the central plain area ranges from 0.159 to 0.922 m. The subsidence of the coastal plain area ranges from 0.211 to 1.921 m. It shows that under the condition of the same amount of exploitation, both area C and area B will produce ground subsidence, but the degree of subsidence of area C is larger than that of area B, i.e. the average subsidence is larger than that of area B. The center of subsidence is located in the coastal plain area. The degree of subsidence in area C is greater than that in area B, i.e., the average amount of subsidence is greater than that in area B, and the center of subsidence is located in the coastal plain area. Although the shallow layer in the coastal plain area also develops a water table landing funnel, the compression contribution of aquifer groups III and IV is superior, i.e., the compression contribution of the deep layer is the largest, because of the change of lithology from the shallow layer to the deep layer, i.e., the transition from fine sand and powder clay to clay, in which the deeper section of clay is larger, i.e., the deeper layer is prone to produce ground compression.

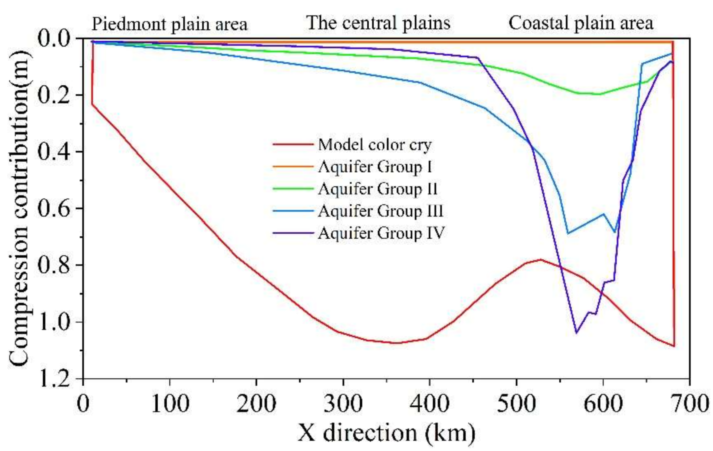

Fig. 10. Scheme 1: Compression curves of each aquifer

Figure 11 shows the compression curves of each aquifer in Scheme 2, and the subsidence in the pre-hill plain area of Scheme 2 ranges from 0.001 to 0.082 m. The subsidence in the central plain area ranges from 0.082 to 0.451 m. The subsidence in the coastal plain area ranges from 0.176 to 1.187 m. The results of the overall scheme show that the average subsidence is greater than that in the central plain area under the condition of shallow groundwater exploitation intensity without considering shallow groundwater exploitation and with the same deep-lying groundwater. Under the condition of groundwater mining intensity, the center of subsidence is located in the coastal plain area, and the average subsidence is larger than that in the central plain area. The percentage of compression contribution of each aquifer is the same as the trend of Scenario 1, and Area C still provides the main compression contributing layer for Aquifer Groups III and IV. However, the cumulative subsidence of each area in Scenario I is higher than that in Scenario II, especially the most obvious change in Area C, which is located in the coastal area, due to the closure of shallow wells.

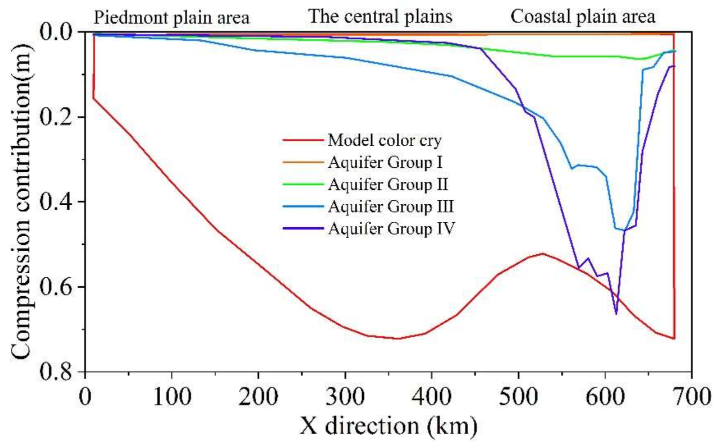

Fig. 11. Scheme 2 Compression curves of each aquifer

Table 6 shows the average subsidence in each area under different pumping schemes, and Figure 12 shows the comparison of vertical displacement in each area under different pumping schemes. By comparing the above two pumping schemes and analyzing the results according to Fig. 12 and Table 6, area C, which is located in the coastal plain, is more likely to produce a groundwater level descent funnel compared with areas B and A. The shallow groundwater extraction scheme has also affected the ground subsidence. Shallow groundwater extraction also has an impact on ground subsidence, and shutting down shallow extraction wells can lead to a significant decrease in total subsidence. Due to the high intensity of shallow mining, resulting in large changes in the water level, when the aquifer in the lower layer of groundwater recharge the shallow aquifer, so the III aquifer group is not only subjected to deep wells, but also need to be recharged to the II aquifer group. The significant decrease in the pore water pressure in the aquifer increases the effective stress, i.e., the compression of the ground layer increases. Therefore, the over-exploitation of shallow groundwater also increases the severity of ground subsidence, but mainly through the compression of the deeper layer, i.e., the deeper layer is still the main layer contributing to the subsidence.

Table 6. Average settlement in different regions under different extraction schemes

Pumping scheme	Average settlement by region (m)		
	A	B	C
Option 1(simultaneous deep and shallow mining)	0.062	0.326	1.229
Option 2Deep mining only)	0.036	0.174	0.718

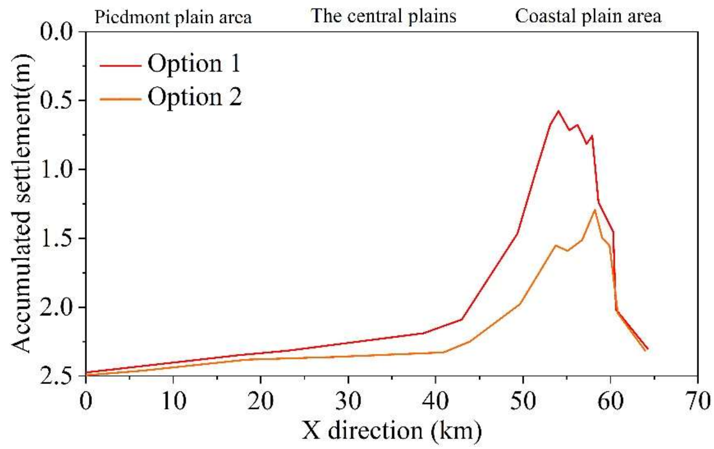

Fig. 12. Comparison of vertical displacement under different schemes

4. Conclusion

In this paper, a coupled model of groundwater flow and soil deformation is constructed based on the theory of fluid-solid coupling, and the model is validated and numerically analyzed by example simulation with the help of MODFLOW simulation software.

1) It is found that the water level in the study area further decreases by November 2021, and the landing funnel shows a trend of outward growth, with a funnel area of 4.32km^2 and a water depth of 54.1m, in addition to a better recognition of soil deformation. Overall, the theoretical simulation analysis results basically coincide with the actual situation in the study area, verifying the reliability of its coupling model.

2) Under the same conditions of deep groundwater extraction, it is concluded that the soil settlement in the mountain front plain area is the smallest (0.001-0.082m), followed by the soil settlement in the mountain front plain area (0.082-0.451m), and the largest is the soil settlement in the coastal plain area (0.176-1.187m), which is due to the over-exploitation of the shallow groundwater that leads to the severity of ground subsidence.

References

[1] Tang, Y., Zhou, J., Yang, P., Yan, J., & Zhou, N. (2017). Groundwater engineering. Springer Singapore.

[2] Patel, A. (2019). Geotechnical investigations and improvement of ground conditions. Woodhead Publishing.

[3] Lipiec, J., Czyż, E. A., Dexter, A. R., & Siczek, A. (2018). Effects of soil deformation on clay dispersion in loess soil. Soil and Tillage Research, 184, 203-206.

[4] Briaud, J. L. (2023). Geotechnical engineering: unsaturated and saturated soils. John Wiley & Sons.

[5] Al-Dakheeli, H., & Bulut, R. (2019). Interrelationship between elastic deformation and soil-water characteristic curve of expansive soils. Journal of Geotechnical and Geoenvironmental Engineering, 145(4), 04019005.

[6] Sultanov, L. U. (2015). Numerical Modelling of Deformation of Soil Foundations. Procedia earth and planetary science, 15, 119-124.

[7] Fern, J., Rohe, A., Soga, K., & Alonso, E. (2019). The material point method for geotechnical engineering: a practical guide. CRC Press.

[8] Pasierb, B., Grodecki, M., & Gwóźdź, R. (2019). Geophysical and geotechnical approach to a landslide stability assessment: a case study. Acta Geophysica, 67(6), 1823-1834.

[9] Zhou, C. B., Chen, Y. F., Hu, R., & Yang, Z. (2023). Groundwater flow through fractured rocks and seepage control in geotechnical engineering: Theories and practices. Journal of Rock Mechanics and Geotechnical Engineering, 15(1), 1-36.

[10] Sun, L., Wang, X., Wang, S., Sun, W., Wang, J., & Di, H. (2024). Experimental study on soil deformation caused by overexploitation of groundwater. Water Environment Research, 96(9), e11111.

[11] He, G., Yan, X., Zhang, Y., Yang, T., Wu, J., Bai, Y., & Gu, D. (2020). Experimental study on the vertical deformation of soils due to groundwater withdrawal. International Journal of Geomechanics, 20(7), 04020076.

[12] Ibrahim, A., & Meguid, M. A. (2020). Coupled flow modelling in geotechnical and ground engineering: an overview. International Journal of Geosynthetics and Ground Engineering, 6(3), 39.

[13] Rahardjo, H., Kim, Y., & Satyanaga, A. (2019). Role of unsaturated soil mechanics in geotechnical engineering. International Journal of Geo-Engineering, 10, 1-23.

[14] Al-Arafat, M., Kabi, M. E., Morshed, A. S. M., & Sunny, M. A. U. (2024). Geotechnical Challenges In Urban Expansion: Addressing Soft Soil, Groundwater, And Subsurface Infrastructure Risks In Mega Cities. Innovatech Engineering Journal, 1(01), 205-222.

[15] Jia, G. S., Ma, Z. D., Xia, Z. H., Wang, J. W., Zhang, Y. P., & Jin, L. W. (2022). Influence of groundwater flow on the ground heat exchanger performance and ground temperature distributions: A comprehensive review of analytical, numerical and experimental studies. Geothermics, 100, 102342.

[16] Ni, P., Mei, G., & Zhao, Y. (2018). Influence of raised groundwater level on the stability of unsaturated soil slopes. International Journal of Geomechanics, 18(12), 04018168.

[17] Lasseux Didier & ValdésParada Francisco J. (2024). Darcy's law survival from no-slip to perfect-slip flow in porous media. Journal of Fluid Mechanics(465),A65-A65.

[18] Idrees Khan,Rozli Zulkifli,T. Chinyoka,Zhi Ling & Murad Ali Shah. (2024). Numerical analysis of radiative MHD gravity-driven thin film third-grade fluid flow with exothermic reaction and modified Darcy's law on an inclined plane. Mechanics of Time-Dependent Materials(1),12-12.

[19] Jiang Fei,Liu Haihu,Chen Xian & Tsuji Takeshi. (2022). A coupled LBM-DEM method for simulating the multiphase fluid-solid interaction problem. Journal of Computational Physics

[20] Zhao Yanan,Liu Hao,Jiang Zhongming,Zhao Hongmin & Mei Songhua. (2023). Two-phase Fluid Solid Coupling Modeling: Theory, Numerical Model, and Application. Journal of Physics: Conference Series(1),

[21] Siu Wun Cheung,Eric T. Chung & Hyea Hyun Kim. (2018). A Mass Conservative Scheme for Fluid-Structure Interaction Problems by the Staggered Discontinuous Galerkin Method. J. Sci. Comput.(3),1423-1456.